International Journal of Heat and Mass Transfer 52 (2009) 3829–3841

Contents lists available at ScienceDirect

International Journal of Heat and Mass Transfer

journal homepage: www.elsevier.com/locate/ijhmt

Slip effects on mixed convective flow and heat transfer from a vertical plate

Kang Cao, John Baker *

Department of Mechanical Engineering, University of Alabama, Box 870276, Tuscaloosa, AL 35487, USA

ARTICLE INFO

Article history:
Received 28 May 2008
Received in revised form 23 January 2009
Available online 15 April 2009

Keywords:
Mixed convection
Slip flow
Vertical plate

ABSTRACT

Laminar mixed convection over an isothermal vertical plate has been modeled with first-order momentum and thermal discontinuities at the wall. Local non-similarity transformations, using two non-similarity variables, have been applied to study the mixed convection boundary layer problem. Numerical solutions were obtained for varying conditions in assisting flow based on the three-equation model. Non-similar velocity and temperature distributions within the boundary layer have been presented. Results are also presented for the effect of non-continuum upon wall slip velocity, temperature jump, wall shear stress and boundary layer thickness in both gaseous and liquid flows for Gr_x/Re_x^2 varying from 0.0001 to 8.0.

1. Introduction

Combined forced and natural convection over a flat plate has been widely studied from both theoretical and experimental standpoints over the past a few decades. Early investigations mainly sought the similarity characteristics within the boundary layer framework. Although the mixed convection problem generally does not admit itself to self-similar solutions, studies have been conducted to examine the conditions under which self-similar solutions do exist in the mixed convection regime. Sparrow et al. [1] examined combined convection about a non-isothermal body with non-uniform free stream velocity. The results showed that similar solutions exist only when free stream velocity and surface temperature vary with distance along the plate as x^m and x^{2m-1}. The criteria for pure and mixed flows were also discussed for both aiding and opposing cases. Schneider [2] examined the mixed convection over a horizontal plate using the first-order boundary layer theory. An exact similarity solution was given for the wall temperature that is inversely proportional to the square root of the distance along the plate. Merkin and Pop [3] also studied the mixed convection boundary layer problem using a similarity method. It was found out that the critical Prandtl number (approximately 0.761) will affect the solution structure in both assisting and opposing flows.

In addition to seeking the exact self-similar solution, other approaches such as asymptotic solutions, local-similarity and perturbation expansion methods, aiming to address a more general mixed convection problem, were also reported in the literature. Oosthuizen and Hart [4] developed a simple implicit finite difference scheme to address the mixed convection over flat plates for both aiding and opposing flows. Numerical results were obtained for cases of uniform temperature and uniform heat flux for Pr of 0.7, 3 and 10. Merkin [5] studied the mixed boundary layer flow over a semi-infinite vertical plate. A series solution was found valid only near the leading edge. A numerical integration method was introduced to extend the solution to the position far downstream where buoyancy force dominates. In addition, flow separation has been shown in the opposing case. Acrivos [6] examined the mixed convection boundary layer flow with the aid of an approximate technique of asymptotic solutions. The result has shown that for large values of Pr the relative importance of the forced and free convection is controlled by $Gr/Re^2Pr^{1/3}$, however, for $Pr \ll 1$ the controlling index is Gr/Re^2. Lloyd and Sparrow [7] employed the local similarity method to transform the boundary-layer equations into a system of ordinary differential equations using the parameter Gr_x/Re_x^2. Numerical solutions were obtained for Pr varying from 0.003 to 100 and Gr_x/Re_x^2 varying from 0 to 4, i.e., spanning from pure forced convection to a strong buoyancy effects. While Gr/Re^2 is conventionally regarded as the appropriate scaling for mixed convection, a few researchers proposed other forms to facilitate the study in various mixed convection problems. Raju [8] introduced two controlling parameters $(1 + Gr^2/Re^4)^{-1}$ and $(1 + Gr^2/Re^5)^{-1}$ to map the entire domain of mixed convection for vertical and horizontal plate, respectively. Results from local similarity and local non-similarity method were presented. It has shown that the former approach provides reasonable estimation for wall friction and Nusselt numbers, while rendering appreciable deviation in velocity profiles compared to the rigorous finite difference solution. Lin and Chen [9] employed the variable $(\sigma Ra)^{1/4}(\omega Re)^{1/2}$ as the controlling parameter in addressing mixed convection over a vertical plate. Finite difference solutions were obtained for Prandtl numbers between 0.001 and 10,000. Zubair and Kadaba [10] investigated the transient mixed convection flow with the aid of a

* Corresponding author. Tel.: +1 205 348 4997; fax: +1 205 348 6419.
E-mail address: john.baker@eng.ua.edu (J. Baker).

0017-9310/$ - see front matter © 2009 Elsevier Ltd. All rights reserved.
doi:10.1016/j.ijheatmasstransfer.2009.02.013

Nomenclature

C_f	skin friction coefficient
c_p	specific heat at constant pressure
f	momentum accommodation coefficient
F	transformed stream function
G	ξ-derivative of F
g	gravitational acceleration
Gr	Grashof number, $Gr = g\beta\Delta TL^3/\nu^2$
H	ξ-derivative of G
h	heat transfer coefficient
k	thermal conductivity
Kn	Knudsen number, $Kn = \lambda/L$
L	characteristic length
Nu	Nusselt number, $Nu = hL/k$
p	pressure
Pr	Prandtl number, $Pr = \mu\ c_p/k$
Re	Reynolds number, $Re = u_\infty L/\nu$
T	temperature
u	streamwise velocity
v	normal velocity
x	coordinate along the plate
y	coordinate normal to the plate

Greek symbols

α	thermal accommodation coefficient
β	volumetric thermal expansion coefficient
γ	specific heat ratio of air
δ	boundary layer thickness
η	pseudo-similarity variable
θ	dimensionless temperature
κ	dimensionless non-continuum variable
λ	mean free path
μ	dynamic viscosity
ν	kinematic viscosity
ξ	controlling parameter of mixed convection
τ	shear stress
φ	ξ-derivative of θ
χ	ξ-derivative of φ
Ψ	stream function

Subscripts

L	length of entire plate
x	local x position
$slip$	slip condition
w	wall boundary
∞	ambient conditions

two-step, group transformation method. Discussion was given on constructing the reduced governing equations and boundary conditions for miscellaneous cases including steady mixed convection, pure steady and unsteady forced and natural convection. Risbeck et al. [11] examined laminar mixed convection over a horizontal plate with a power-law variation of surface temperature, i.e., $T(x) = T_\infty + ax^n$. Based on a weighted finite difference solution, the results showed that both local wall heat flux and wall shear stress will increase with the increasing value of n for a given Pr. For additional information on prior studies of mixed convection behavior, the reader may wish to consult the book by Gebhart et al. [12].

The majority of previous studies were conducted within the continuum regime. Nonetheless, as the mean free path of the flow becomes comparable to the characteristic length scale of the problem, the flows will start to exhibit non-continuum phenomena as a result of fewer molecular collisions within the dimension of interest. The deviation from interfacial thermodynamic equilibrium will lead to a flow regime where the conventional no-slip wall condition is not valid. According to the value of Knudsen number, the flows can be classified into three categories: continuum flow ($Kn < 0.01$), slip flow ($0.01 \leqslant Kn \leqslant 0.1$) and transitional flow ($0.1 < Kn < 10$) [13]. As the flow deviates away from the continuum limit, the conventional no-slip wall boundary condition fails to accurately model the surface interaction between the fluid and the wall boundary due to the low collision frequency [13]. Slip models have been proposed to ameliorate the prediction of the non-continuum phenomenon near wall boundaries within the framework of the continuum assumption. For gaseous flows, the Maxwell slip model relates the slip velocity at the wall to the local velocity gradient based on the gas kinetic theory, given by [14]

$$u_{slip} \approx \left(\frac{2}{f} - 1\right)\lambda\left.\frac{du}{dy}\right|_w \tag{1}$$

For liquid slip flows, the linear Navier boundary condition provides an empirical model relating the slip velocity at the wall to the local shear rate by [14]

$$u_{slip} \approx l_s\left.\frac{du}{dy}\right|_w \tag{2}$$

where l_s is the slip length. It has been found that the slip length depends on the liquid, the flow geometry and the shear rate [14]. An experimental study by Tretheway and Meinhart [15] has found that the slip length for water flowing over a hydrophobic surface is approximately 1 μm.

In addition to velocity slip, as the Knudsen number grows beyond the continuum limit, a temperature jump may exist between the gas molecules and the wall boundary. An interfacial temperature discontinuity physically accounts for gas molecules not thermally accommodated with the wall and thus is very important to the prediction of energy transfer. Analogous to velocity slip, the kinetic theory expression for a first-order temperature jump condition is given by [14]

$$T_{slip} - T_w \approx \left(\frac{2}{\alpha} - 1\right)\frac{2\gamma}{\gamma+1}\frac{\lambda}{Pr}\left.\frac{dT}{dy}\right|_w \tag{3}$$

Over the past two decades, studies have examined both gaseous and liquid internal flows at microscales. A brief summary of previous studies can be found in the literature [16–21]. Nonetheless, the literature on external convective flow with slip boundary conditions is found to be very limited. Oosthuizen [22] roughly estimated the effects of very small amounts of slip (with Kn varying from 10^{-5} to 10^{-4}) on the free convection from a vertical plate using the Von Karman integral approach. A slight increase was predicted in the average Nusselt number with the increasing slip condition. Eldighidy and Fathalah [23] examined the effect of momentum slip on natural convection from a vertical plate. Temperature jump, however, was not considered in the boundary condition. The results indicated that velocity and heat transfer at the plate will be enhanced with increasing Kn. Martin and Boyd [24] investigated the forced convection over a horizontal plate with slip conditions. Numerical solutions were obtained using finite difference methods. Results suggested that the flow structure, velocity profile, and boundary layer thickness will be altered by the rarified condition. To the authors' knowledge,

no previous study has been undertaken to examine the simultaneous momentum and thermal slip effect upon mixed convection, though the interfacial discontinuity is important in predicting the flow and heat transfer behavior at slightly rarefied conditions.

The aim of this study is to provide a better understanding of the effect interfacial velocity and temperature discontinuity have upon combined forced and natural convection. This paper provides local non-similar solutions to the boundary-layer equations for mixed convection over a vertical isothermal plate in a slightly rarefied environment. Simultaneous velocity slip and temperature jump boundary conditions were considered for gaseous slip flow. The variations in velocity and temperature distributions, wall shear stress and boundary layer thickness with the condition of interfacial slip have been analyzed in gases. A correlation of skin friction coefficient and average heat transfer, i.e., Nusselt number, over the plate has been formulated in an integral form as a function of the non-continuum parameter and the thermophysical properties of the flow.

2. Mixed convection with interfacial slip

A schematic illustration and coordinate system of the mixed convection over an isothermal vertical plate is shown in Fig. 1, where T_s and T_∞ denote the uniform temperature of plate surface and the ambient temperature respectively, and u_∞ is uniform free stream velocity. When $T_s > T_\infty$, the flow is designated as aiding flow since buoyancy effects have a positive component with the free stream velocity. On the other hand if $T_s < T_\infty$, it is designated as opposing flow as buoyancy effects are in the opposite direction with the free stream velocity.

The governing equations for laminar, steady and incompressible flow are, respectively, the continuity, momentum and energy equations. Assumptions are also made that viscous dissipation is neglected and that the variation of fluid properties is taken to be negligible except for the essential density variation appearing in the gravitational body force. Therefore the resulting equations for the present two-dimensional problem are given by

$$\frac{\partial u}{\partial x}+\frac{\partial v}{\partial y}=0 \tag{4}$$

$$\rho\left(u\frac{\partial u}{\partial x}+v\frac{\partial u}{\partial y}\right)=-\frac{\partial p}{\partial x}+\mu\left(\frac{\partial^2 u}{\partial x^2}+\frac{\partial^2 u}{\partial y^2}\right)\pm\rho g \tag{5}$$

$$\rho\left(u\frac{\partial v}{\partial x}+v\frac{\partial v}{\partial y}\right)=-\frac{\partial p}{\partial y}+\mu\left(\frac{\partial^2 v}{\partial x^2}+\frac{\partial^2 v}{\partial y^2}\right) \tag{6}$$

$$\rho c_p\left(u\frac{\partial T}{\partial x}+v\frac{\partial T}{\partial y}\right)=k\left(\frac{\partial^2 T}{\partial x^2}+\frac{\partial^2 T}{\partial y^2}\right) \tag{7}$$

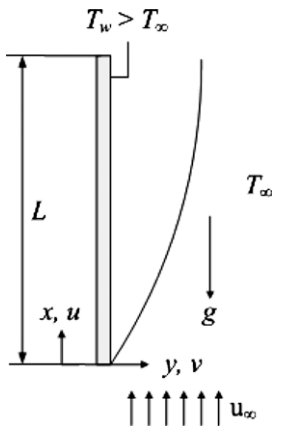

Fig. 1. Mixed convection over a vertical plate.

With the boundary layer assumption and Boussinesq approximation [25], Eqs. (4) through (7) are reduced to the boundary-layer equations

$$u\frac{\partial u}{\partial x}+v\frac{\partial u}{\partial y}=\pm g\beta(T-T_\infty)+\upsilon\frac{\partial^2 u}{\partial y^2} \tag{8}$$

$$u\frac{\partial T}{\partial x}+\upsilon\frac{\partial T}{\partial y}=\alpha\frac{\partial^2 T}{\partial y^2} \tag{9}$$

The positive sign in Eq. (8) applies in buoyancy assisting flow while the negative sign applies in opposing flow.

A group of dimensionless parameters are introduced to seek the local non-similar solutions including a pseudo-similarity position parameter η, dimensionless stream function F and dimensionless temperature θ, which are defined as

$$\eta=y(u_\infty/\nu x)^{1/2} \tag{10}$$

$$F(\xi,\eta)=\psi/(u_\infty \nu x)^{1/2} \tag{11}$$

$$\theta(\xi,\eta)=(T-T_\infty)/(T_w-T_\infty) \tag{12}$$

In addition, another dimensionless variable usually employed as a controlling index to characterize the relative importance of free convection to forced convection is defined as

$$\xi=Gr_x/Re_x^2 \tag{13}$$

ξ can span from 0 to ∞, corresponding to the two limiting cases of pure forced convection and pure natural convection, respectively. When ξ is approximately unity, effects from natural and forced convection are comparable. Note that ξ is in proportional to x. Therefore, the initial boundary layer flow is dominated by forced convection, but as the distance from leading edge increases, the contribution of free convection will become prominent.

2.1. Interfacial slip boundary conditions

First consider the wall boundary conditions for gaseous flow within slip regime. Two interfacial discontinuities involving momentum and energy transfer, given by Eqs. (1) and (3), are used to replace the no-slip conditions applied for non-rarefied flows. In light of the defined dimensionless variables, the momentum and thermal boundary conditions at the wall can be transformed to the dimensionless forms as

$$F'(0)=\left(\frac{2}{\sigma}-1\right)Kn_x Re_x^{1/2}F''(0) \tag{14}$$

$$\theta(0)=\left(\frac{2}{\alpha}-1\right)\frac{1}{Pr}Kn_x Re_x^{1/2}\frac{2\gamma}{\gamma+1}\theta'(0)+1 \tag{15}$$

where prime denotes the derivative with respective to η. Kn_x and Re_x are, respectively, the local Knudsen number, and local Reynolds number. γ is 7/5 for a diatomic gas, 5/3 for a monatomic gas, and approximately 1.0 for a liquid [14]. f is defined as the ratio of diffuse reflections to the total number of reflections, and α is the fraction of impinging molecules which becomes accommodated to the temperature of the wall. Experiments have shown that the momentum and thermal accommodation coefficients are fairly close to unity for rough surfaces where molecules are reflected by the wall at random angles [14]. On a microscale level, even a highly polished surface can be viewed as rough for molecules. f and α are therefore assumed to be of unity in this study, i.e., we have assumed diffuse reflection and complete thermal accommodation between the molecules and the wall.

Note that the above slip conditions are dependent upon the streamwise location x. In this regard, a non-similarity variable ξ is defined to describe the surface location dependence of x

$$\kappa=Kn_x Re_x^{1/2} \tag{16}$$

Similarly, in liquid flows, the Navier slip boundary conditions based on Eq. (2) can be transformed to

$$F'(0) = \left(\frac{2}{f} - 1\right)\frac{l_s}{x}\mathrm{Re}_x^{1/2}F''(0) \tag{17}$$

Accordingly the slip parameter for liquid flows has the form

$$\kappa = \frac{l_s}{x}Re_x^{1/2} \tag{18}$$

where $\frac{l_s}{x}$ may be viewed as the dimensionless local slip length for liquid flows.

Although κ is different for gaseous and liquid flows, it bears similar physical meanings for both. First, the value of κ is proportional to $x^{-1/2}$ and hence it describes the streamwise location along the plate. Second, κ controls the slip boundary conditions for both flows. The magnitude of κ can be used to describe the degree of non-continuum condition at the wall, or in other words, how much the flow deviates from the no-slip condition. For instance, if κ is zero it indicates that the x location is far downstream from the leading edge of the plate where the slip effect will be negligible. On the other hand, a larger value of κ indicates that the boundary condition will deviate more from the no-slip case. As κ approaches infinity, the velocity slip and temperature jump at the wall will become infinity large, giving a nearly uniform velocity and temperature distribution with the ambient condition:

$$F'(0) = 1, \quad \theta(0) = 0 \quad \text{as } \kappa \to \infty \tag{19}$$

It should be noted that for a very large value of κ that corresponds to a very small x at the leading edge, the boundary layer assumption is not appropriate, and as a consequence, the boundary-layer equations become inaccurate. Moreover, if a large κ is due to a Knudsen number greater than 0.1, then the Navier–Stokes equation fails to model the transitional or even free molecule flow regime. For this reason, a discussion regarding large value κ could be prone to error in nature. We therefore limit the discussion in this paper to a relatively small range of κ from 0 to 5 as this will cover the slip flow region.

In addition to the two slip boundary conditions, the other boundary conditions including impermeable wall, the ambient velocity and the ambient dimensionless temperature θ are

$$v_w = 0, \quad u_\infty = 0, \quad \theta_\infty = 0 \tag{20}$$

The latter two conditions in Eq. (20) are equivalent to

$$F' = 0, \quad \theta = 0 \quad \text{as } \eta \to \infty \tag{21}$$

The mathematical expression for the normal velocity at the plate, however, needs more consideration as will be seen shortly in the following subsection.

2.2. Formulation of boundary-layer equations

It has been noted that mixed convection does not generally admit similar solutions due to the effect of buoyancy upon forced convection. For the present problem, the non-similarity aspect also arises from the presence of slip at the wall boundary. With the two non-similarity variables ξ and κ being dependent upon the streamwise location along the plate, it suggests that the reduced stream function F, temperature distribution θ and their derivatives will also be a functions of the streamwise location. The first step of the analysis is to transform from (x,y) coordinates to (ξ,η). Note the coordinate ξ is dependent only on x while η is a function of both y and x. Accordingly, the reduced stream function can be modified to be $F(\xi,\eta)$ and the dimensionless temperature $\theta(\xi,\eta)$. With the modified definitions, the longitudinal and normal velocity components can be derived as

$$u = \frac{\partial\psi}{\partial y} = u_\infty F'(\kappa,\eta) \tag{22}$$

$$v = -\frac{\partial\psi}{\partial x} = -\frac{\partial}{\partial x}\left[F(\kappa,\eta)(u_\infty \nu x)^{1/2}\right] = \frac{1}{2}\sqrt{\frac{u_\infty \nu}{x}}\left(\eta F' + \kappa\frac{\partial F}{\partial\kappa} - F\right) \tag{23}$$

Therefore, the dimensionless velocity components may be defined as

$$u^* = u/u_\infty = F'(\xi,\eta) \tag{24}$$

$$V^* = \frac{v}{(1/2)\sqrt{\nu u_\infty/x}} = \eta F' + \kappa\frac{\partial F}{\partial\kappa} - F \tag{25}$$

In terms of the above relations, the governing equations of Eqs. (8) and (9) can be transformed as

$$F''' + \frac{1}{2}FF'' \pm \xi\theta = \xi\left(F'\frac{\partial F'}{\partial\xi} - F''\frac{\partial F}{\partial\xi}\right) \tag{26}$$

$$\frac{1}{Pr}\theta'' + \frac{1}{2}F\theta' = \xi\left(F'\frac{\partial\theta}{\partial\xi} - \theta'\frac{\partial F}{\partial\xi}\right) \tag{27}$$

With the normal velocity v expressed in Eq. (25), the boundary condition of v_w is given by

$$F = \kappa\frac{\partial F}{\partial\kappa}, \quad \text{at } \eta = 0 \tag{28}$$

The other boundary conditions are stated in Eqs. (14), (15), (19), and (21).

2.3. Local-similarity model

Before proceeding into the local non-similarity method, it is useful to examine the boundary-layer equations Eqs. (8) and (9) from the perspective of local similarity concept. To derive the equations for local similarity model, one assumes that the terms on the right side of Eqs. (26)–(28) are sufficiently small so that they may be neglected. Then the local similarity transformation is given by

$$F''' + \frac{1}{2}FF''^2 \pm \xi\theta = 0 \tag{29}$$

$$\frac{1}{Pr}\theta'' + \frac{1}{2}F\theta' = 0 \tag{30}$$

Accordingly, the boundary conditions for local similarity transformation are

$$\begin{cases} F(0) = 0 \\ F'(0) = \kappa F''(0) \\ \theta(0) = \frac{\kappa}{Pr}\frac{2\gamma}{\gamma+1}\theta'(0) + 1 \\ F'(\xi,\infty) = 1, \qquad \theta(\xi,\infty) = 0 \end{cases} \tag{31}$$

The parameter ξ and κ contained in the governing equations and boundary conditions can be regarded as assigned constant values at any streamwise location along the plate. As a result, the governing equations transformed by the local similarity method can be treated as a system of ordinary differential equations, with partial non-similar effects retained in the momentum equation and the boundary conditions. For a given value of ξ and κ, the solution is independent of other streamwise locations. Therefore, by assigning a succession of ξ and κ values along the plate, the velocity and temperature distributions can be determined.

Nevertheless, the comparatively simplified solution is at the expense of uncertain accuracy. During the local-similarity transformation, the non-similar terms on the right side of Eqs. (26) and (27), i.e., parts of the momentum and energy equations, were lost. The local similarity postulation requires ξ be close to zero which is

valid for negligible buoyancy effects. Otherwise, the whole terms in bracket on right side of Eqs. (26) and (27) must be very small to justify the exclusion of non-similar terms. The validity of the latter assumption, however, is subject to uncertainty and thus is a weakness of the local-similarity method. The local-similarity concept discussed above represents the first step in a succession of local non-similarity transformations.

2.4. Local non-similarity models

In order to overcome the limitations imposed by local-similarity method, the local non-similar boundary-layer equations will now be derived. The two-equation model will be first derived. Let

$$G(\xi,\eta)=\partial F(\xi,\eta)/\partial\xi,\quad \varphi(\xi,\eta)=\partial\theta(\xi,\eta)/\partial\xi \tag{32}$$

Note also that the two similarity variables ξ and η are both a function of x and they are related by

$$d\kappa/d\xi=-\kappa/2\xi \tag{33}$$

Differentiating Eqs. (26) and (27) with respect to ξ, gives the set of auxiliary equations

$$G'''+\frac{1}{2}FG''-F'G'+\frac{3}{2}F''G\pm\xi\varphi\pm\theta=\xi\frac{\partial}{\partial\xi}(F'G'-F''G) \tag{34}$$

$$\frac{1}{Pr}\varphi''+\frac{1}{2}F\varphi'-F'\varphi+\frac{3}{2}G\theta'=\xi\frac{\partial}{\partial\kappa}(F'\varphi-\theta'G) \tag{35}$$

Similarly, the additional boundary conditions can be obtained by differentiating Eqs. (14), (15), (21), and (28) with respective to ξ

$$\begin{cases} G(0)=-\frac{2}{3}\xi\frac{\partial}{\partial\xi}G(0)\\ G'(0)=-\frac{\kappa}{2\xi}F''(0)+\kappa G''(0)\\ \varphi(0)=\frac{1}{Pr}\frac{2\gamma}{\gamma+1}\left[-\frac{\kappa}{2\xi}\theta'(0)+\kappa\varphi'(0)\right]\\ G'(\xi,\infty)=0,\qquad \varphi(\xi,\infty)=0 \end{cases} \tag{36}$$

If the right side terms containing $\xi\partial/\partial\xi$ in Eqs. (34) and (35) are neglected, then they become as the subsidiary momentum and energy equations for Eqs. (26) and (27). In a likely manner, Eq. (36) is auxiliary boundary conditions to the original ones. This is referred to as the two-equation model since the momentum and energy distribution each involves the solution to two simultaneous equations.

The above outlined procedures represent the first stage of the local non-similarity model. The governing equations for the three-equation model can be formulated in a similar manner to the two-equation model. First let

$$H(\xi,\eta)=\partial G/\partial\xi,\quad \chi(\xi,\eta)=\partial\varphi/\partial\xi \tag{37}$$

Then Eqs. (34)–(36) are differentiated with respect to ξ and neglect the terms containing $\xi\partial^2/\partial\xi^2$ This transformation yields a second set of auxiliary equations and boundary conditions

$$H'''+\frac{1}{2}FH''-2F'H'+\frac{5}{2}F''H+3GG''-2(G')^2\pm\xi\chi\pm2\varphi=0 \tag{38}$$

$$\frac{1}{Pr}\chi''+\frac{1}{2}F\chi'-2F'\chi+3G\varphi'-2G'\varphi+\frac{5}{2}H\theta'=0 \tag{39}$$

$$\begin{cases} H(0)=0\\ H'(0)=\frac{3\kappa}{4\xi^2}F''(0)-\frac{\kappa}{\xi}G''(0)+\kappa H''(0)\\ \chi(0)=\frac{1}{Pr}\frac{2\gamma}{\gamma+1}\left[\frac{3\kappa}{4\xi^2}\theta'(0)-\frac{\kappa}{\xi}\varphi'(0)+\kappa\chi'(0)\right]\\ H'(\xi,\infty)=0,\qquad \chi(\xi,\infty)=0 \end{cases} \tag{40}$$

In summary, all the momentum and energy equations for the three-equation model are brought together as

$$F'''+\frac{1}{2}FF''\pm\xi\theta=\xi\left(F'\frac{\partial F'}{\partial\xi}-F''\frac{\partial F}{\partial\xi}\right) \tag{41a}$$

$$\frac{1}{Pr}\theta''+\frac{1}{2}F\theta'=\xi\left(F'\frac{\partial\theta}{\partial\xi}-\theta'\frac{\partial F}{\partial\xi}\right) \tag{41b}$$

$$G'''+\frac{1}{2}FG''-F'G'+\frac{3}{2}F''G\pm\xi\varphi\pm\theta=\xi(G'G'+F'H'-G''G-F''H) \tag{41c}$$

$$\frac{1}{Pr}\varphi''+\frac{1}{2}F\varphi'-F'\varphi+\frac{3}{2}G\theta'=\xi(G'\varphi+F'\chi-\varphi'G-\theta'H) \tag{41d}$$

$$H'''+\frac{1}{2}FH''-2F'H'+\frac{5}{2}F''H+3GG''-2(G')^2\pm\xi\chi\pm2\varphi=0 \tag{41e}$$

$$\frac{1}{Pr}\chi''+\frac{1}{2}F\chi'-2F'\chi+3G\varphi'-2G'\varphi+\frac{5}{2}H\theta'=0 \tag{41f}$$

The three-equation model involves six coupled momentum and energy equations that need to be solved simultaneously in conjunction with a set of boundary conditions. Although the solution to the three-equation model provides information on six parameters, it is only F and θ and their derivatives that are of primary interest since they are the ones meaningful to the physical problem. The above transformed governing equations are identical to those reported in [26] since the general mixed convection regardless of the presence of slip is also dependent on streamwise locations. The effect of momentum and thermal discontinuity are reflected in the boundary conditions in Eqs. (31), (36) and (40).

The local non-similarity transformation preserves the non-similar terms in original governing equations and boundary conditions with only part of the subsidiary non-similar terms dropped from its subsidiary equations. Since the original governing equations remain intact, the local non-similarity method is expected to be more accurate than the local-similarity solution. In addition, since the non-similar terms are only dropped at the level of the secondarily subsidiary momentum and energy equations, the results from the three-equation model should have higher accuracy than those from the two-equation model. The reader may also wish to consult the literature [27,28] for more discussion regarding the numerical accuracy of the local non-similarity method.

3. Results and discussion

The system of ordinary differential equations for the local non-similarity three-equation model represents a two-point boundary value problem and needs to be solved simultaneously. The equations were solved numerically using the three-stage Lobatto IIIA collocation method that provides continuous solutions of fourth-order accuracy uniformly in the problem domain. The numerical algorithm, application procedures and validation of accuracy have been outlined in great detail in [29,30], so they will not be repeated here.

Numerical solutions were obtained for mixed convection in only the assisting case for present study. Results from the three-equation non-similarity model are presented for velocity and temperature distribution, wall slip velocity, wall shear stress, skin friction coefficient and average Nusselt number over the plate.

3.1. Effect of slip in gaseous flows

Mixed convection with slip is first considered for assisting flow in gases. Fig. 2 shows the representative velocity profiles for $Pr = 0.72$ in assisting mixed flows at varying rarefaction conditions. At κ equal to 0, Fig. 2(a) shows the velocity distribution at the no-slip condition. In the case of a very weak buoyancy effect, e.g., $\xi = 0.0001$, the result is very close to the pure forced convection. For example, $F'(\eta)$ is less than 1% variation with the classical Blasius solution [14]. It is also seen From Fig. 2(a)–(d), that the

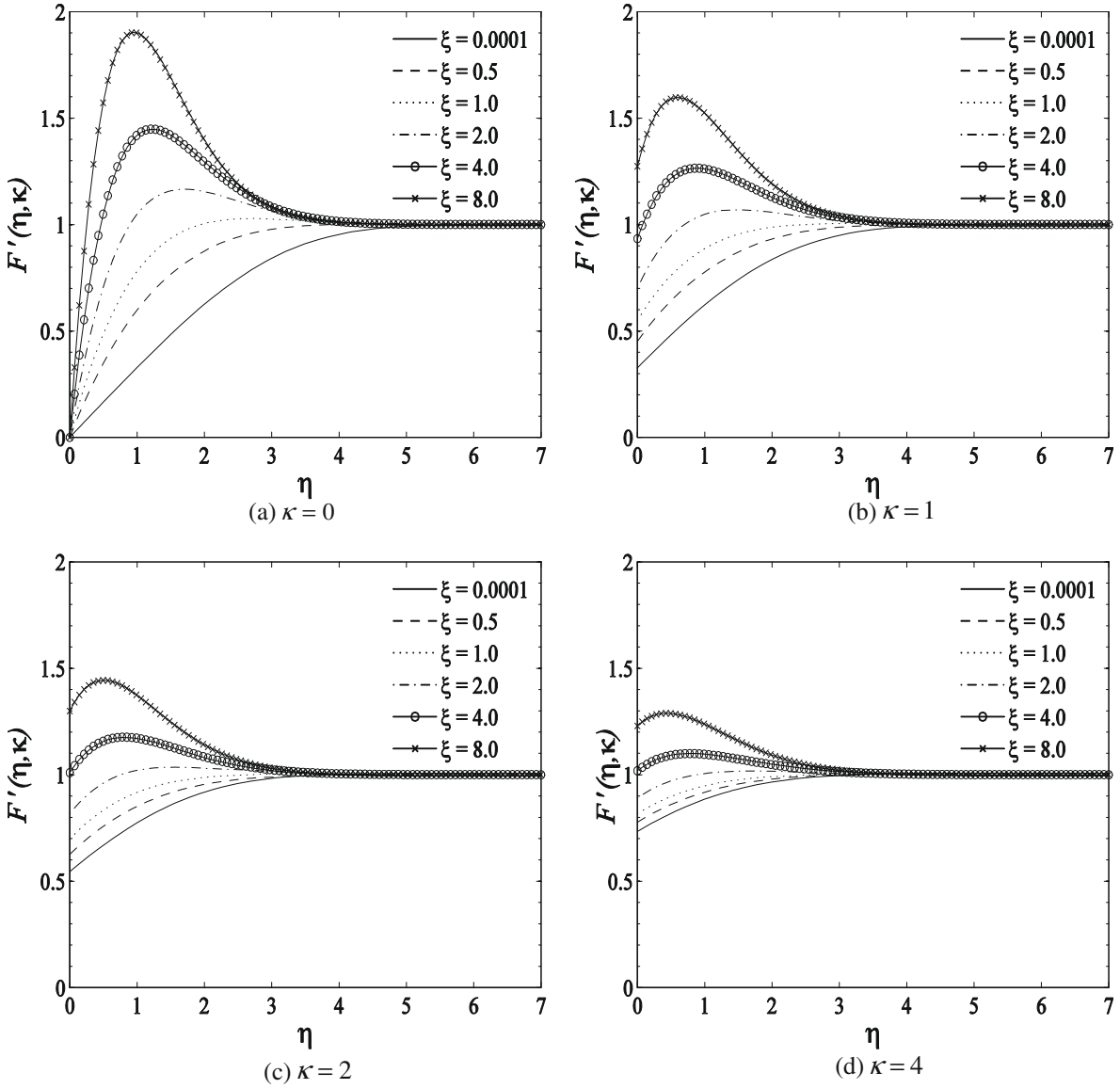

Fig. 2. Representative velocity profile from three-equation model ($Pr = 0.72$).

velocity profile in the vicinity of plate will be greatly altered due to the presence of non-continuum at the wall. In forced convection dominated flows i.e., $\xi \leqslant 0.5$, the slip velocity at the wall increases with the increasing non-continuum condition. In flow with strong buoyancy effects i.e., $\xi \geqslant 2.0$, the peak velocity in the boundary layer is seen to decrease with the increasingly rarefied condition, causing approximately 30% and 12% decrease respectively for ξ of 2.0 and 8.0 as κ varies from 0 to 4.0. Note also the position η at which the peak velocity attains will shift toward the plate as the flow becomes more rarefied.

The wall slip velocity $F'(0)$ as a function of non-continuum for Pr of 0.72 is shown in Fig. 3. The slip velocity is seen to increase with increasing buoyancy effects. The slip velocity will reach approximately 78% of the free stream velocity for ξ of 0.0001 and 120% for ξ of 8.0 as κ approaches 5, which indicates the flow is accelerated by natural convection near the plate. It is also interesting to note that in the buoyancy dominated flows, i.e., $\xi = 8.0$, the slip velocity tends to decrease after reaching a peak value rather than monotonically increase with the increased rarefaction. For instance, in mixed flow with $\xi = 8.0$, $F'(0)$ initially increases with the rarefaction reaching a peak value of 1.308 at κ equal to 1.7.

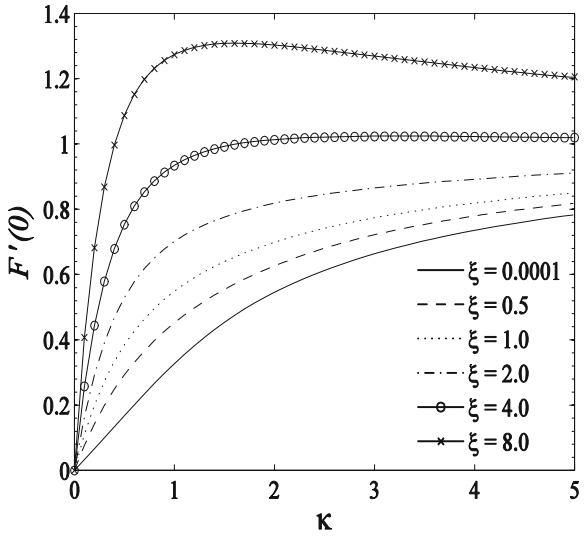

Fig. 3. Wall slip velocity as a function of non-continuum.

The slip velocity begins to decrease slowly as the flow becomes further rarefied, giving about 9% drop below the peak value as κ approaches 5.0. This behavior is due to the growing effect of natural convection in the mixed flows. It can be justified by a closer examination of the second boundary condition in Eq. (31), which indicates the wall slip velocity will attain its peak value when the product of non-continuum κ and the dimensionless skin friction $F''(0)$ is maximized, as is seen shortly.

Skin friction coefficient is one of the physical quantities of interest in evaluating the viscous stress acting on the surface the plate. The wall shear stress can be expressed as

$$\tau_w = \mu \frac{\partial u}{\partial y}\bigg|_{y=0} = \frac{\mu u_\infty}{x} Re_x^{1/2} F''(0) \tag{42}$$

Hence then the local friction coefficient has the form

$$C_{f,x} = \frac{\tau_{w,x}}{\rho u_\infty^2/2} = 2Re_x^{-1/2} F''(0) \tag{43}$$

The dimensionless skin friction $F''(0)$ is shown in Fig. 4. The result shows that for a given ξ, $F''(0)$ has the maximum value at the no-slip condition and the wall shear stress will decrease as the flow becomes more rarefied. In addition, a faster percentage drop of $F''(0)$ is found in buoyancy dominated flows. For instance, $F''(0)$ decreases by approximately 75% for ξ at 8.0 and 45% for ξ of 0.5, as κ varies from 0 to 1.0. Note also at this point, the behavior of wall slip velocity can be examined closely. As noticed earlier, the peak slip velocity $F'(0)$ will occur when the product of κ and $F''(0)$ is maximized. From geometric reasoning, $\kappa F''(0)$ represents the rectangle area encompassed by respective coordinate for an arbitrary point on the curve shown in Fig. 4. Therefore, the maximum wall slip velocity is attained when this area is maximized. It has also been shown in the figure that $F''(0)$ is 0.3322 at ξ equal to 0.0001. The wall shear stress differs only 0.05% from the classical Blasius solution at the no-slip condition.

The local wall shear stress at the no-slip condition is compared to the results reported by Merkin [5] for the cases of ξ varying from 0.00001 to 10.190. Note that for direct comparison, the results presented in Table 1 are based on Pr of 1.0, which is the same Prandtl number used by Merkin. Note $W(\xi)$ in the table is defined as $\frac{C_{f,x}}{2Re_x^{-1/2}\xi^{1/2}}$. It is seen that for no-slip condition, the local wall shear stress based on the three-equation model agrees reasonably well with the published data in [5]. The maximum difference is about 2% at ξ of 10.190. The differences between the results obtained in this study and those reported by Merkin [5] are seen to increase

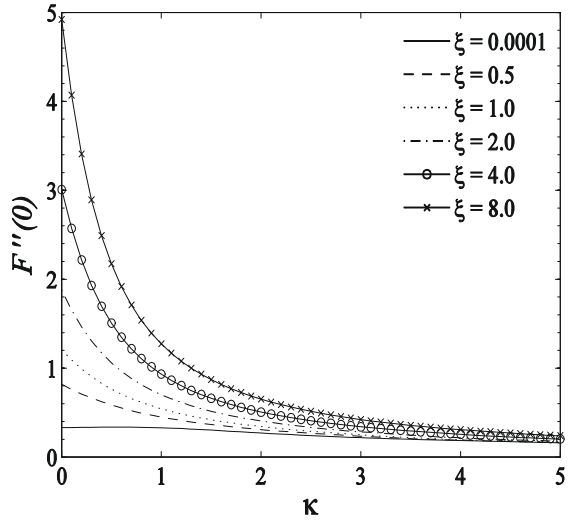

Fig. 4. Skin friction as a function of non-continuum (Pr = 0.72).

Table 1
Comparison of local wall stress at the no-slip condition (Pr = 1.0).

ξ	$W(\xi)$	$W(\xi)$ [5]
0.00001	105.0	105.0
0.00448	5.038	5.038
0.04928	1.742	1.742
0.10048	1.388	1.388
0.20288	1.197	1.196
0.30528	1.143	1.142
0.46912	1.123	1.120
0.55104	1.124	1.121
0.67392	1.131	1.127
0.79680	1.142	1.137
0.87872	1.150	1.145
1.00000	1.164	1.157
1.2815	1.195	1.186
1.5375	1.223	1.213
2.1007	1.281	1.268
2.5103	1.320	1.304
4.0463	1.441	1.419
5.2751	1.520	1.494
10.190	1.751	1.714

gradually as ξ increases. The difference between the two set of results may be attributed to the nature of the numerical methods used in respective study. For the non-similarity methods, parts of the non-similar terms are dropped from the subsidiary boundary-layer equations during the transformation processes. While the omitted terms may have negligible effects in numerical accuracy for small ξ values, inaccuracy will be introduced as ξ increases especially to large values. On the other hand, the results reported by Merkin [5] were obtained by matching the results of a numerical integration with the asymptotic series solutions at far down stream. The potential numerical inaccuracy for this method includes truncation error in the series solutions as well as the difference approximation used for the numerical integration. The reader may wish to consult [5] for more information about the numerical accuracy.

The total viscous drag force per unit width can be computed by integrating the wall shear stress over the entire plate of length L

$$F_D = \int_0^L \tau_w dx = \rho \upsilon^{1/2} u_\infty^{3/2} \int_0^L x^{-1/2} F''(0) dx \tag{44}$$

The drag coefficient is defined as [25]

$$C_D = F_D / \left(\frac{1}{2} \rho u_\infty^2 L \right) \tag{45}$$

After substituting the definition of non-continuum parameter κ in to Eq. (44), and changing the integration with respect to κ, the expression for the drag coefficient is

$$C_D / Re_L^{-1/2} = 4\kappa_L \int_{\kappa_L}^{\infty} F''(\xi, 0) \kappa^{-2} d\kappa \tag{46}$$

where κ_L is the non-similarity variable κ evaluated at length L. Note Eq. (46) is similar to the integral form of drag coefficient for pure forced convection in rarefied flows reported in [24]. The integrand $F''(\xi,0)$ is however different than that for the pure force convection since it is also a function of the mixed convection parameter. As seen in Fig. 4, for a given Prandtl number and ξ, $F''(0)$ varies with the non-continuum condition κ. The functional relation between $F''(0)$ and κ may be obtained by curve fitting. Take ξ of 1.0 and Pr of 0.72, for instance, $F''(0)$ may be correlated by

$$\frac{C_{f,x}}{2Re_x^{-1/2}} = \frac{3.314}{2.728 + 3.288\kappa^{1.029}}, (Pr = 0.72,\ \xi = 1.0) \tag{47}$$

The coefficient of determination of the above equation is 0.9999. The drag coefficient $\frac{C_D}{Re_L^{-1/2}}$ was obtained by substituting Eq. (47) into

Eq. (46) for numerical integration. The drag coefficient as a function of non-continuum for *Pr* of 0.72 and ξ of 1.0 is plotted in Fig. 5. The result shows that the drag coefficient decreases rapidly with the increasing non-continuum condition, giving approximately 90% drop as κ_L varies from 0 to 5.0.

The boundary layer thickness is given by

$$\delta = x\eta_b Re_x^{-1/2} \tag{48}$$

For mixed flows, the freestream velocity is superimposed by the velocity component from the natural convection. Hence the conventional definition of boundary thickness for forced and natural convection does not apply directly for mixed flows. The viscous boundary layer thickness, however, may be defined from the standpoint of the shear stress, i.e., the value of η where the magnitude of $F'(\eta) = 0.01$. The expression of boundary layer thickness can be substituted into the definition of κ in Eq. (16) to obtain,

$$\kappa = Kn_\delta \eta_b \tag{49}$$

Eq. (49) indicates that the effect of slip is a function of boundary layer thickness. The value of η_b as a function of ξ for varying non-continuum conditions is shown in Fig. 6. It is interesting to note the general trend that the viscous boundary layer thickness will first decease to a localized minimum value and then increase with the increasing buoyancy effects. This behavior is due to the effect that natural convection enhances the velocity field near the plate. It is also seen that the boundary layer thickness decreases as the flow becomes more rarefied. This behavior suggests that the transition to turbulence in gaseous flows could be delayed as the flow in rarefied flows.

Fig. 7 shows the dimensionless temperature profile θ for *Pr* of 0.72 with varying ξ at differing non-continuum conditions. It is seen that the amount of thermal jump at the wall will increase monotonically as the flow being more rarefied, giving an average of 80% decrease relative to the no-slip value as κ varies from 0 to 4.0. The dimensionless wall temperature as a function of non-continuum for *Pr* of 0.72 is shown in Fig. 8. The amount of temperature drop is greater as the buoyancy effects become stronger. Note also the decreasing rate in temperature is more drastic at the initial stage of rarefaction, for instance, it causes more than a 45% reduction in $\theta(0)$ for ξ at 1.0 when κ varies from the no-slip condition to 1.0. The result indicates that a small thermal jump condition at the wall boundary can have a remarkable impact on the temperature distribution within the boundary layer.

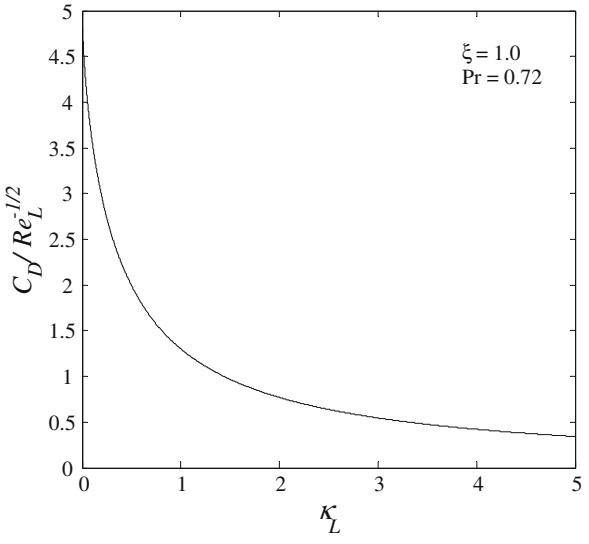

Fig. 5. Drag coefficient as a function of non-continuum (*Pr* = 0.72).

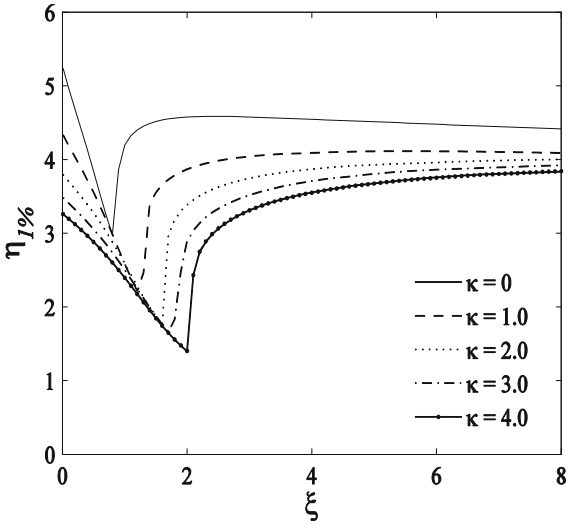

Fig. 6. Viscous boundary layer thickness (*Pr* = 0.72).

The dimensionless local heat transfer is proportional to the magnitude of the local temperature gradient on the plate, given by $\frac{Nu_x}{Re_x^{1/2}} = -\theta'(\xi, 0)$. The local heat transfer at the plate as a function of the mixed convection parameter and the non-continuum parameter is plotted in Fig. 9. The results show that the heat transfer tends to decrease as the flow becomes more rarefied, causing an about 80% decrease for ξ of 8.0 and 65% for ξ of 0.001, as κ varies from 0 to 5.0. This behavior is due to the effect of the simultaneous velocity slip and thermal jump conditions imposed at the wall. Although it is expected that the enhanced velocity due to slip near the plate will increase the local heat transfer, the existing wall temperature jump plays a counteractive role in decreasing the heat transfer. The attenuation in heat transfer caused by the thermal jump condition outweighs the increased amount caused by the slip velocity, thereby resulting in a decreasing local heat transfer with rarefaction. It is also seen that the local heat transfer is greater in the natural convection dominated flows at slightly rarefied conditions, i.e., $\kappa < 1$. However, the heat transfer in flows with strong buoyancy effects is seen to decrease more rapidly with the increasing non-continuum than in weak buoyancy flows. At highly rarefied conditions, the heat transfer rate is less affected by the buoyancy effects, causing only 2% difference between ξ of 0.001 and 8.0 at $\kappa = 5.0$.

The local heat transfer $\frac{Nu_x}{Re_x^{1/2}}$ at the no-slip condition is compared to the results reported in [5] for ξ varying from 0.00001 to 10.190. The results tabulated in Table 2 are based on *Pr* of 1.0. Note $Q(\xi)$ is defined as $\frac{Nu_x}{Re_x^{1/2}\xi^{1/2}}$. It is seen that the local heat transfer at no-slip condition from the three-equation model agrees reasonably well with the results in [5], giving a maximum difference of about 1.8% at ξ of 10.190.

The average Nusselt number over the entire plate is an important physical quantity of interest in quantifying heat transfer behavior. The average heat transfer coefficient can be defined as

$$\bar{h} = \frac{1}{L}\int_0^L h dx = \frac{k}{L}\left(\frac{u_\infty}{\nu}\right)^{1/2}\int_0^L -\theta'(\xi,0)x^{-1/2}dx \tag{50}$$

Then the average Nusselt number over the entire plate is given by

$$\overline{Nu}_L = \left(\frac{u_\infty}{\nu}\right)^{1/2}\int_0^L -\theta'(\xi,0)x^{-1/2}dx \tag{51}$$

As seen in Fig. 9, the wall temperature gradient $\theta'(\xi,0)$ (or the local heat transfer) can be viewed as a function of κ as well due to the interfacial non-continuum. In terms of the definition of κ, the average Nusselt number can be derived as an integral form

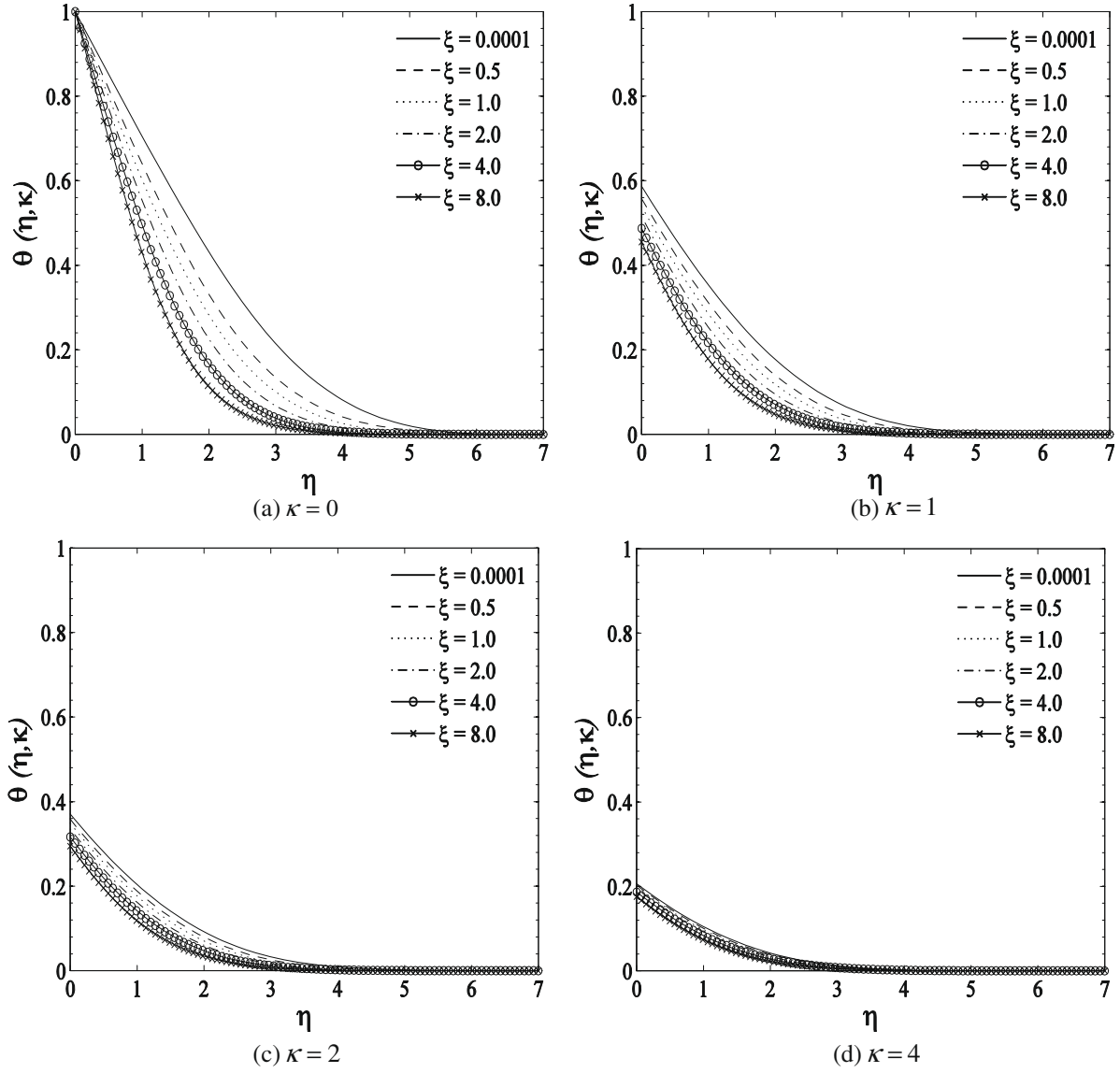

Fig. 7. Temperature profile from three-equation model ($Pr = 0.72$).

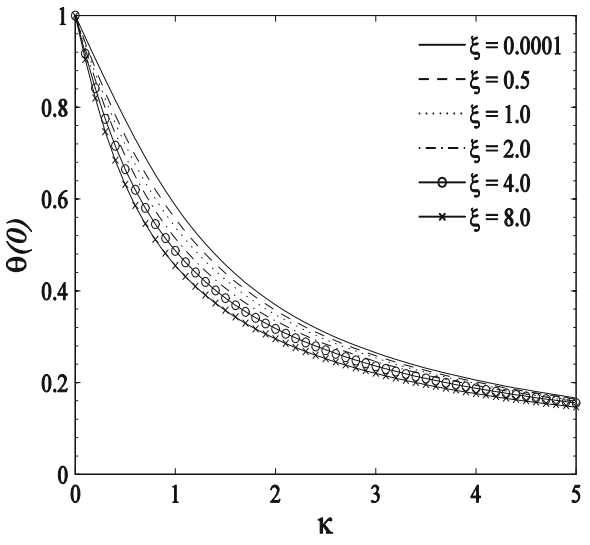

Fig. 8. Wall temperature as a function of non-continuum ($Pr = 0.72$).

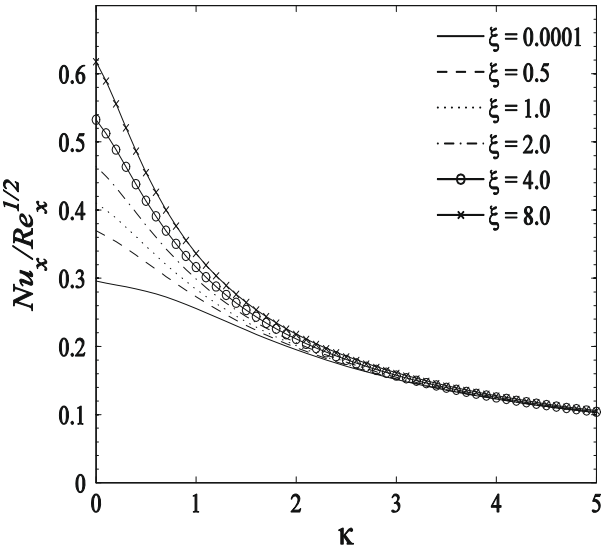

Fig. 9. Local heat transfer as a function of non-continuum ($Pr = 0.72$).

Table 2
Comparison of local heat transfer at the no-slip condition (Pr = 1.0).

ξ	$Q(\xi)$	$Q(\xi)$ [5]
0.00001	105.0	105.0
0.00448	4.978	4.978
0.04928	1.552	1.552
0.10048	1.122	1.122
0.20288	0.8311	0.8315
0.30528	0.7058	0.7066
0.46912	0.5998	0.6011
0.55104	0.5656	0.5672
0.67392	0.5265	0.5284
0.79680	0.4967	0.4989
0.87872	0.4804	0.4827
1.00000	0.4599	0.4624
1.2815	0.4237	0.4266
1.5375	0.3996	0.4028
2.1007	0.3623	0.3659
2.5103	0.3430	0.3468
4.0463	0.2976	0.3018
5.2751	0.2756	0.2799
10.190	0.2290	0.2334

$$\overline{Nu}_L/Re_L^{1/2} = 2\kappa_L \int_{\kappa_L}^{\infty} -\theta'(\xi,0)\kappa^{-2} d\kappa \tag{52}$$

where $\kappa_L = Kn_L Re_L^{1/2}$. Note also Eq. (50) is similar to the average Nusselt number for pure forced convection reported in [24]. It is due to the fact that both the mixed convection and non-continuum parameter are dependent upon the streamwise location. The integrand $\theta'(\xi,0)$ contained in Eq. (52) however differs than that for pure forced convection for it is also a function of the mixed convection parameter. For a given Prandtl number and mixed convection condition, the temperature gradient varies with κ only. The expression of $-\theta'(\xi,0)$ therefore may be obtained fitting the curve to κ. Take Pr of 0.72 and ξ of 1.0 for example, the wall temperature gradient can be related as a function of the non-continuum through

$$\frac{Nu_x}{Re_x^{1/2}} = \frac{2.145}{5.166 + 2.403\kappa^{1.179}} \tag{53}$$

The above correlation gives a coefficient of determination of 0.9997. The average Nusselt number was then obtained by substituting the above expression into Eq. (52) for numerical integration and the result is plotted in Fig. 10. It is evident that the heat transfer will decrease significantly with the increasingly rarefied condition, giving more than 85% decrease in average Nusselt number as the flow varies from the no-slip condition to highly rarefied at κ equal to 5.0. The foregoing procedures can be repeated to determine the average Nusselt number at an arbitrary mixed convection condition of ξ, provided the curve fitting process and numerical integration are of acceptable accuracy.

3.2. Effect of slip in liquid flows

The foregoing discussion has focused on the effect of simultaneous momentum and thermal interfacial discontinuity in gaseous mixed convection. Our discussion in this section is extended to the effects of slip upon mixed convection in liquids. As heat transfer is concerned for slip flow in liquids, it is usually assumed that there is no wall temperature jump accompanying with the momentum slip [24]. Thus, the temperature at the wall is still the no-slip condition $\theta(0) = 0$. Other boundary conditions remain unaltered. Numerical solutions were obtained for Pr of 7.0 in assisting flow with differing non-continuum conditions.

Fig. 11 shows the representative velocity profiles for Pr of 7.0 in assisting flow as a function of non-continuum and mixed conditions. Similar to that in gaseous flows, the velocity distribution near the plate is significantly affected by the degree of rarefaction.

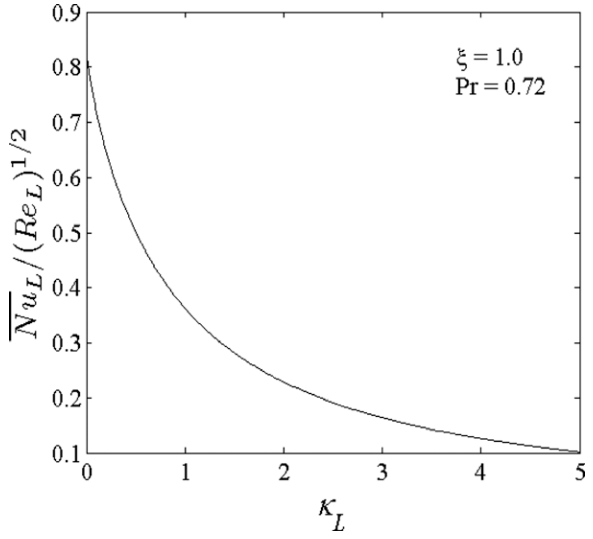

Fig. 10. Average Nusselt number as a function of non-continuum (Pr = 0.72).

Increases are predicted in both wall slip velocity and the peak velocity in buoyancy dominated flows as the flow becomes increasingly rarefied.

The wall slip velocity $F'(0)$ as a function of non-continuum for Pr of 7.0 is shown in Fig. 12. The slip velocity at the plate increases monotonically as the flow becomes more rarefied. In addition, the slip velocity tends to increase with the increasing buoyancy effects. Note $F'(0)$ reaches approximately 78% of the free stream velocity for ξ of 0.0001 and 200% for ξ of 8.0, as κ approaches 5. The buoyancy effects are shown to enhance the slip velocity at the plate as the flow becomes more rarefied.

Fig. 13 shows the dimensionless wall shear stress for Pr of 7.0. The result shows that $F''(0)$ will decrease with the as the flow becomes more rarefied. It is also seen that in buoyancy dominated flows the wall shear stress decreases more rapidly, i.e., $F''^{(0)}$ decreases by approximately 60% for ξ at 8.0 and 30% for ξ at0.5, as κ varies from 0 to 1.0.

Fig. 14 shows the local heat transfer on the plate as a function of the non-continuum parameter for Pr of 7.0. Note the local heat transfer is equal to the value of $-\theta'(\xi,0)$. The result shows that the local heat transfer will be greatly enhanced by the increased rarefaction condition in liquid flows. For instance, the increase in $\frac{Nu_x}{Re_x^{1/2}}$ is approximate 77% for ξ of 8.0 and 105% for ξ of 0.001. Although the local heat transfer is greater at larger ξ, the percentage of change is more significant in buoyancy dominated flows, indicating the velocity slip has a greater impact on heat transfer in flows with less buoyancy effects.

By the same procedure illustrated in the preceding subsection, the average Nusselt number over the entire plate can be obtained by integrating Eq. (52). For example, with ξ of 1.0 and Pr of 7.0, the temperature gradient may be correlated with non-continuum by

$$\frac{Nu_x}{Re_x^{1/2}} = \frac{0.6431 + \kappa^{1.066}}{0.7495 + 0.5464\kappa^{1.092}} \tag{54}$$

This correlation gives a determination of 0.999993. The results for average Nusselt number are plotted in Fig. 15. The result shows that the heat transfer over the entire plate will increase significantly with the increasingly rarefied condition, giving more than 100% increase in the average Nusselt number as the flow varies from the no-slip condition to highly rarefied at κ equal to 5.0. It is also interesting to notice that the heat transfer behavior in rarefied liquid flow is contrary to that in gases, as seen in Fig. 10. In liquids, the velocity slip boundary condition leads to an increased velocity field

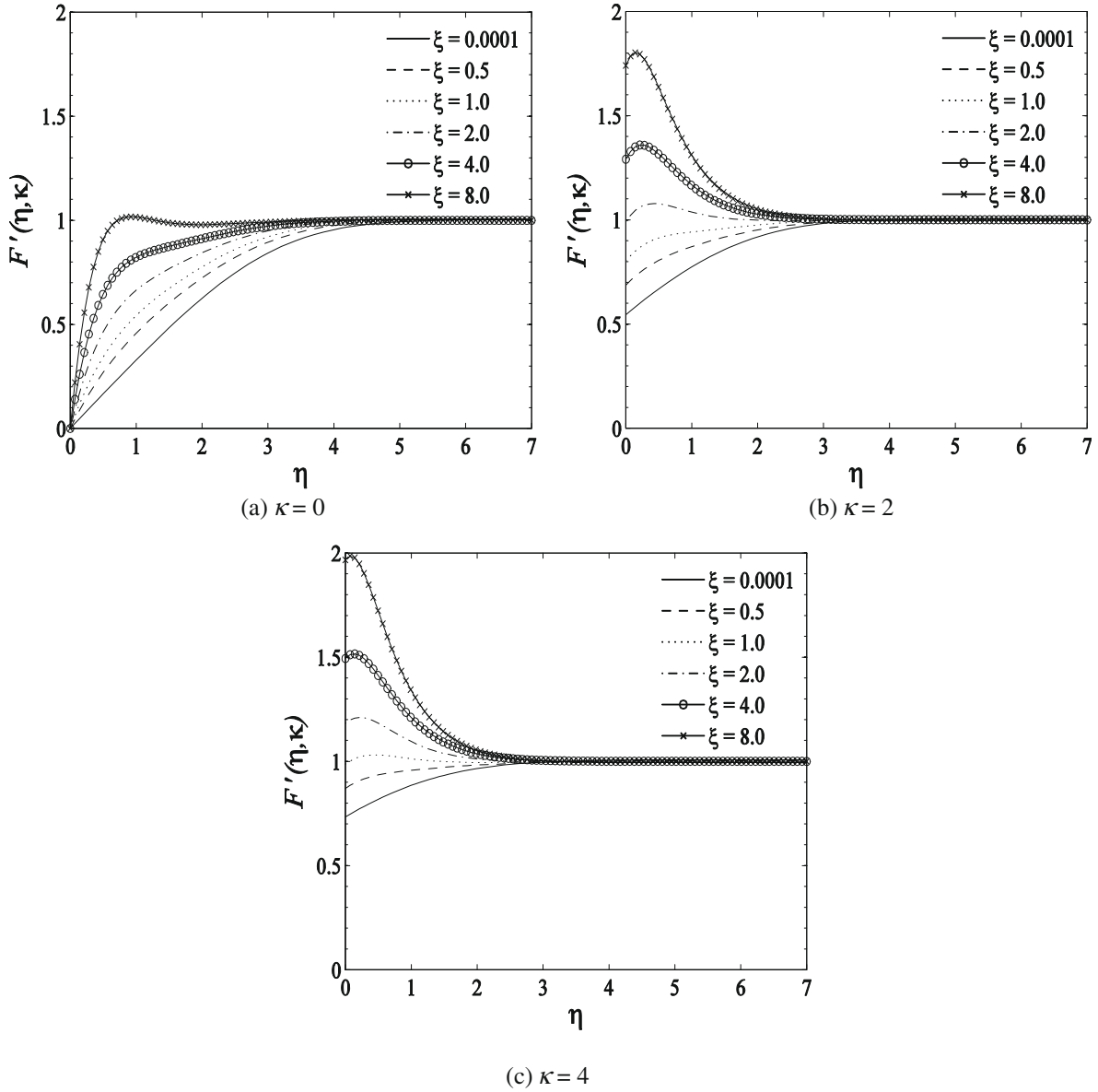

(a) $\kappa = 0$ (b) $\kappa = 2$

(c) $\kappa = 4$

Fig. 11. Velocity profile as a function of κ and ξ ($Pr = 7.0$).

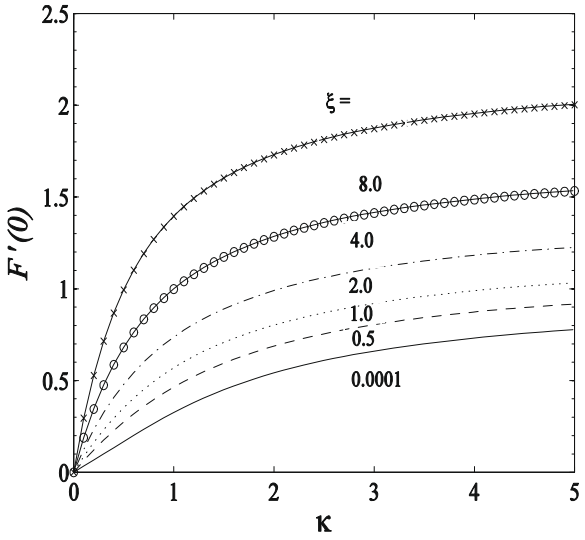

Fig. 12. Wall slip velocity as a function of non-continuum ($Pr = 7.0$).

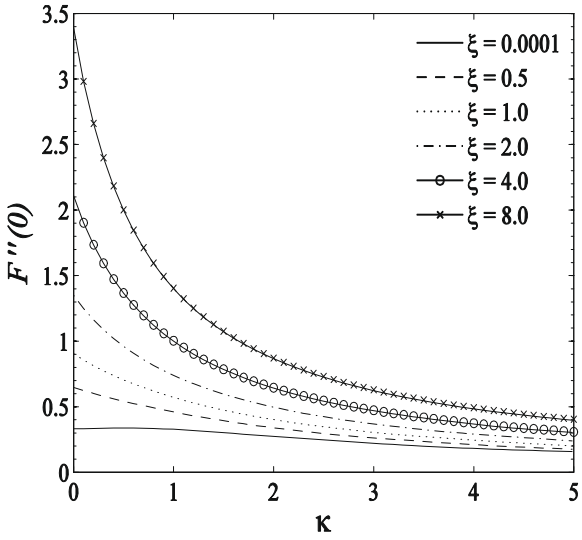

Fig. 13. Wall shear stress as a function of non-continuum ($Pr = 7.0$).

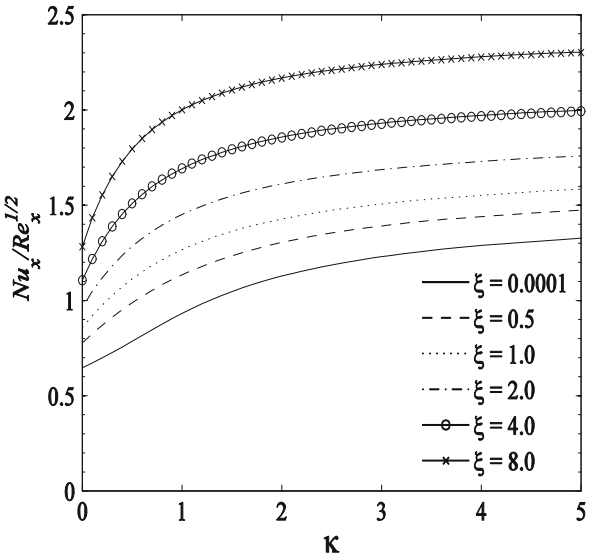

Fig. 14. Local heat transfer as a function of non-continuum ($Pr = 7.0$).

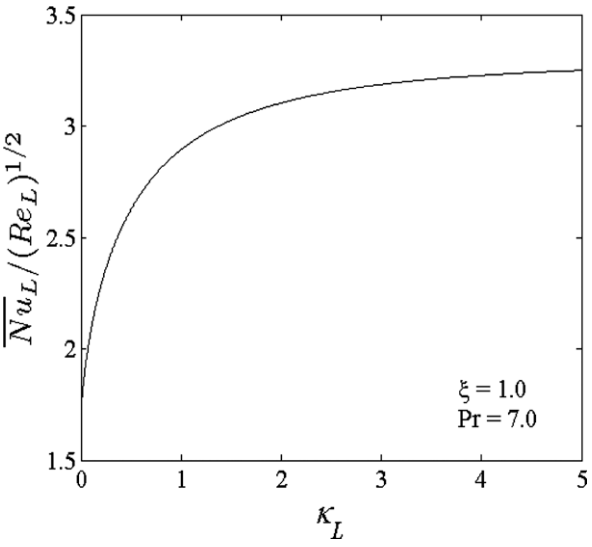

Fig. 15. Average Nusselt number as a function of non-continuum ($Pr = 7.0$).

near the plate. As a result, heat transfer from the plate will be enhanced due to the increased velocity field as the flow becomes more rarefied. Nevertheless, in gaseous flows, the presence of thermal jump condition at the wall will significantly mitigate the heat transfer from the plate. It also turns out that the decreased heat transfer due to the presence of thermal jump offsets more than that gained by the velocity slip, thereby leading to a reduced heat transfer in gaseous slip flows.

4. Conclusion

The boundary-layer equations for mixed convection over a vertical flat plate have been solved with first-order interfacial slip boundary conditions using local non-similarity transformations. The mixed rarefied flows are found to be governed by two non-similarity variables: mixed convection controlling index ξ and non-continuum condition κ. Numerical solutions based on the three-equation model have been obtained for mixed convection in assisting flows for Prandtl numbers of 0.72 and 7.0, respectively. For each Prandtl number, the mixed convection parameter was varied from 0.0001 to 8.0 allowing the buoyancy forces to vary from weak to dominating. Non-similar velocity and temperature distributions within boundary layer have been shown for a wide range of non-continuum conditions. In buoyancy dominated gaseous flows, a peak slip velocity exists in moderately rarefied condition, i.e., the maximum wall slip velocity reaches 1.308 at κ equal to 1.7 for ξ of 8.0. In liquid flows, the wall slip velocity however is found to increase monotonically as the flow becomes more rarefied. The slip boundary condition results in a rapid decrease in wall shear stress below the no-slip value. For instance at ξ of 1.0, $F''(0)$ decreases by more than 85% in gas flow ($Pr = 0.72$) and 75% in liquid ($Pr = 7.0$) as κ varies from 0 to 5. In addition, the decrease in wall shear stress is found to be more substantial in stronger buoyancy flows.

The heat transfer in the boundary layer is also affected by the presence of interfacial slip boundary conditions. In liquid slip flows, the heat transfer is augmented greater than the no-slip value as a result of the momentum slip. In gaseous flows, however, the heat transfer decreases as the flow becomes more rarefied. This behavior is due to the fact that temperature jump condition reduces the heat transfer more than that enhanced by the wall slip velocity.

In addition, the integral formulation of the drag coefficient Eq. (46) and average Nusselt number Eq. (52) as a function of non-continuum conditions are useful for the analysis of mixed convective flow in microscale configurations or at slightly rarefied environments.

Acknowledgments

This work has been supported by The University of Alabama's College of Engineering through the Alton Scott Research Working Group Program and also by a University Graduate Council Fellowship. The authors acknowledge the Alabama Space Grant Consortium, whose initial support for the undergraduate balloonsat program at The University of Alabama motivated this work.

References

[1] E.M. Sparrow, R. Eichhorn, J.L. Gregg, Combined forced and free convection in a boundary layer flow, Phys. Fluids 2 (3) (1959) 319–328.
[2] W. Schneider, A similarity solution for combined forced and free convection flow over a horizontal plate, Int. J. Heat Mass Transfer 22 (10) (1979) 1401–1406.
[3] J.H. Merkin, I. Pop, Mixed convection along a vertical surface: similarity solutions for uniform flow, Fluid Dyn. Res. 30 (4) (2002) 233–250.
[4] P.H. Oosthuizen, R. Hart, A numerical study of laminar combined convective flow over flat plates, J. Heat Transfer 95 (1) (1973) 60–63.
[5] J.H. Merkin, The effect of buoyancy forces on the boundary-layer flow over a semi-infinite vertical flat plate in a uniform free stream, J. Fluid Mech. 35 (3) (1969) 439–450.
[6] A. Acrivos, On the combined effect of forced and free convection heat transfer in laminar boundary layer flows, Chem. Eng. Sci. 21 (4) (1966) 343–352.
[7] J.R. Lloyd, E.M. Sparrow, Combined forced and free convection flow on vertical surfaces, Int. J. Heat Mass Transfer 13 (2) (1970) 434–438.
[8] M.S. Raju, X.Q. Liu, C.K. Law, A formulation of combined forced and free convection past horizontal and vertical surfaces, Int. J. Heat Mass Transfer 27 (12) (1984) 2215–2224.
[9] H.T. Lin, C.C. Chen, Mixed convection on vertical plate for fluids of any Prandtl number, Heat Mass Transfer 22 (1988) 159–168.
[10] S.M. Zubair, P.V. Kadaba, Similarity transformations for boundary layer equations in unsteady mixed convection, Int. Commun. Heat Mass Transfer 17 (2) (1990) 215–226.
[11] W.R. Risbeck, T.S. Chen, B.F. Armaly, Laminar mixed convection over horizontal flat plates with power-law variation in surface temperature, Int. J. Heat Mass Transfer 36 (7) (1993) 1859–1866.
[12] B. Gebhart, Y. Jaluria, R.L. Mahajan, B. Sammakia, Buoyancy-Induced Flows and Transport, Hemisphere Publishing Corporation, New York, 1988. Textbook ed., (Chapter 3).
[13] M. Gad-el-Hak, The fluid mechanics of microdevices – the freeman scholar lecture, J. Fluids Eng. 121 (1) (1999) 5–33.

[14] F.M. White, Viscous Fluid Flow, third ed., McGraw-Hill, New York, 2006 (Chapters 1 and 4).
[15] D.C. Tretheway, C.D. Meinhart, Apparent fluid slip at hydrophobic microchannel walls, Phys. Fluids 14 (3) (2002) L9–L12.
[16] C.M. Ho, Y.C. Tai, Micro-electro-mechanical-systems (MEMS) and fluid flows, Ann. Rev. Fluid Mech. 30 (1) (1998) 579–612.
[17] M.G. Mala, D. Li, Flow characteristics of water in microtubes, Int. J. Heat Fluid Flow 20 (2) (1999) 142–148.
[18] N.T. Obot, Toward a better understanding of friction and heat/mass transfer in microchannels – a literature review, Microscale Thermophys. Eng. 6 (3) (2002) 155–173.
[19] J. Koo, C. Kleinstreuer, Liquid flow in microchannels: experimental observations and computational analyses of microfluidics effects, J. Micromech. Microeng. 13 (5) (2003) 568–579.
[20] H.A. Stone, A.D. Stroock, A. Ajdari, Engineering flows in small devices: microfluidics toward a lab-on-a-chip, Ann. Rev. Fluid Mech. 36 (2004) 381–411.
[21] C. Neto, D.R. Evans, E. Bonaccurso, H.-J. Butt, V.S.J. Craig, Boundary slip in Newtonian liquids: a review of experimental studies, Reports on Progress in Physics 68 (12) (2005) 2859–2897.
[22] P.H. Oosthuizen, The effect of surface slip on the laminar free convective heat transfer from an isothermal vertical flat plat, Appl. Sci. Res. 16 (1) (1966) 121–130.
[23] S.M. Eldighidy, K.A. Fathalah, Effect of the slip boundary condition on natural convection heat transfer from an isothermal vertical plate, J. Eng. Appl. Sci. 1 (2) (1981) 129–138.
[24] M.J. Martin, I.D. Boyd, Momentum and heat transfer in a laminar boundary layer with slip flow, J. Thermophys. Heat Transfer 20 (4) (2006) 710–719.
[25] F.P. Incropera, D.P. DeWitt, Introduction to Heat Transfer, fourth ed., Wiley, 2001 (Chapter 9).
[26] W.J. Minkowycz, E.M. Sparrow, G.E. Schneider, R.H. Pletcher, Handbook of Numerical Heat Transfer, Wiley, New York, 1988 (Chapter 5).
[27] E.M. Sparrow, H. Quack, C.J. Boerner, Local nonsimilarity boundary-layer solutions, AIAA J. 8 (11) (1970) 1936–1942.
[28] E.M. Sparrow, H.S. Yu, Local non-similarity thermal boundary-layer solutions, J. Heat Transfer 93 (4) (1971) 328–334.
[29] J. Kierzenka, L.F. Shampine, A BVP solver based on residual control and the MATLAB PSE, ACM Trans. Math. Softw. 27 (3) (2001) 299–316.
[30] L.F. Shampine, I. Gladwell, S. Thompson, Solving ODEs with MATLAB, Cambridge University Press, 2003 (Chapter 3).